Cortical phase-amplitude coupling is key to the occurrence and treatment of freezing of gait

Zixiao Yin,[1,2,†] Guanyu Zhu,[1,2,†] Yuye Liu,[1,2,†] Baotian Zhao,[1,2] Defeng Liu,[1,2] Yutong Bai,[1,2] Quan Zhang,[1,2] Lin Shi,[1] Tao Feng,[3] Anchao Yang,[1] Huanguang Liu,[1] Fangang Meng,[2,4] Wolf-Julian Neumann,[5] Andrea A. Kühn,[5,6,7] Yin Jiang[2,4] and Jianguo Zhang[1,2,4]

[†]**These authors contributed equally to this work.**

1 Department of Neurosurgery, Beijing Tiantan Hospital, Capital Medical University, Beijing, China

2 Department of Functional Neurosurgery, Beijing Neurosurgical Institute, Capital Medical University, Beijing, China

3 Department of Neurology, Beijing Tiantan Hospital, Capital Medical University, Beijing, China

4 Beijing Key Laboratory of Neurostimulation, Beijing, China

5 Movement Disorder and Neuromodulation Unit, Department of Neurology, Charité - Campus Mitte, Charite – Universitatsmedizin Berlin, Chariteplatz 1, 10117 Berlin, Germany

6 Berlin School of Mind and Brain, Charite – Universitatsmedizin Berlin, Unter den Linden 6, 10099 Berlin, Germany

7 NeuroCure, Charite – Universitatsmedizin Berlin, Chariteplatz 1, 10117 Berlin, Germany

Correspondence to: Prof. Dr Jianguo Zhang

Capital Medical University, Department of Neurosurgery, Beijing Tiantan Hospital, No. 119 South 4th Ring West Road, Fengtai District, 100070, Beijing, China

E-mail: zjguo73@126.com

Correspondence may also be addressed to: Dr Yin Jiang

Capital Medical University, Department of Functional Neurosurgery, Beijing Neurosurgical Institute, No. 119 South 4th Ring West Road, Fengtai District, 100070, Beijing, China.

jiangyin0802@foxmail.com

Running title: Cortical PAC explains the pathology of FOG

Abstract

Freezing of gait is a debilitating symptom in advanced Parkinson's disease and responds heterogeneously to treatments such as deep brain stimulation. Recent studies indicated that cortical dysfunction is involved in the development of freezing, while evidence depicting the specific role of the primary motor cortex in the multi-circuit pathology of freezing is lacking. Since abnormal beta-gamma phase-amplitude coupling recorded from the primary motor cortex in patients with Parkinson's disease indicates parkinsonian state and responses to therapeutic deep brain stimulation, we hypothesized this metric might reveal unique information on understanding and improving therapy on freezing of gait.

Here we directly recorded potentials in the primary motor cortex using subdural electrocorticography and synchronously captured gait freezing using optoelectronic motion-tracking systems in 16 freely-walking patients with Parkinson's disease who received subthalamic nucleus deep brain stimulation surgery. Overall, we recorded 451 timed up-and-go walking trials, and quantified 7,073 s of stable walking and 3,384 s of gait freezing in conditions of ON/OFF-stimulation and with/without dual-tasking.

We found that (i) high beta-gamma phase-amplitude coupling in the primary motor cortex was detected in freezing trials (i.e., walking trials that contained freezing), but not nonfreezing trials, and the high coupling in freezing trials was not caused by dual-tasking or the lack of movement; (ii) nonfreezing episodes within freezing trials also demonstrated abnormally high couplings, which predicted freezing severity; (iii) deep brain stimulation of subthalamic nucleus reduced these abnormal couplings and simultaneously improved freezing; and (iv) in trials that were at similar coupling levels, stimulation trials still demonstrated lower freezing severity than no-stimulation trials.

These findings suggest that elevated phase-amplitude coupling in the primary motor cortex indicates higher probabilities of freezing. Therapeutic deep brain stimulation alleviates freezing by both decoupling cortical oscillations and enhancing cortical resistance to abnormal coupling. We formalized these findings to a novel "bandwidth model," which specifies the role of cortical dysfunction, cognitive burden, and therapeutic stimulation on the emergence of freezing. By targeting key elements in the model, we may develop next-generation deep brain stimulation approaches for freezing of gait.

Keywords: Parkinson's disease; deep brain stimulation; freezing of gait; motor cortex; phase amplitude coupling

Abbreviations: DBS = deep brain stimulation; ECoG = electrocorticography; FI = freezing index; FOG = freezing of gait; HFS = high frequency stimulation; LME = linear mixed effect; LFS = low frequency stimulation; PAC = phase-amplitude coupling; PSD = power spectral density; STN = subthalamic nucleus; UPDRS = Unified Parkinson's Disease Rating Scale

Introduction

Freezing of gait (FOG), defined as the "episodic absence or marked reduction of forward motion of feet despite the intention to walk"[1], is one of the most debilitating symptoms in Parkinson's disease[2,3]. Although deep brain stimulation (DBS) of the subthalamic nucleus (STN) well controls cardinal symptoms of Parkinson's disease such as tremor and motor fluctuation, current DBS therapy provides modest and highly heterogeneous benefits to FOG[4–8]. Revealing the neurophysiological patterns directly associated with FOG and the underlying modulation effects induced by DBS will foster optimized DBS therapy targeting FOG.

As a higher-level modulator of the supraspinal locomotor network, the primary motor cortex (M1) participates in the control of gait initiation and gait stability[9,10]. Previous structural MRI and magnetic resonance spectroscopy studies indicated that a lower gray matter volume and abnormal metabolite ratios were evident in the M1 of subjects with freezing/impaired gait[9,11]. By leveraging functional MRI and virtual reality gait paradigms, Shine et al.[12] observed a significant decrease in blood oxygen level-dependent response in the bilateral M1 during behavioural freezing compared to stable walking. Since neuroimaging studies were unable to model real gait during scanning, Pozzi et al.[13] recently recorded multisite neurophysiological signals (STN and scalp EEG) during walking, and found that FOG was associated with low frequency decoupling between motor cortex regions and the STN, further confirming the involvement of dysfunctional M1 in FOG. However currently, the neurophysiological characteristics specifically related to FOG within the M1 remain largely unknown. In addition, little attention has been paid to the influence of DBS in improving FOG and the corresponding underlying cortical response. This knowledge, though can be challenging to get, is particularly important for translating current findings into improved DBS therapy, e.g., adaptive DBS targeting freezing[14].

Recent research has identified abnormal beta-gamma phase-amplitude coupling (PAC) in the M1 as a cortical biomarker of parkinsonian motor impairment that can be reversed through therapeutic DBS[15]. PAC has been hypothesized as a physiological mechanism for neural intra- and inter-region communication by coordinating the timing of spiking and synaptic inputs[16], while excessive PAC may constrain information transmission[17]. Since FOG also involves dysfunction in M1, and is characterized as a disorder associated with impaired neural transmission efficiency in the locomotion system[18], we hypothesized that PAC in M1

might reveal unique information on mechanisms underlying the emergence and treatment of FOG in Parkinson's disease.

In this study, we recorded subdural electrocorticographic (ECoG) signals directly from the M1 of freely-walking patients with Parkinson's disease who received STN-DBS therapy. Through synchronized three-dimensional (3D) optoelectronic motion tracking systems, we quantified long periods of stable walking and ongoing freezing in both the stimulation OFF and ON states. We observed that the intensity of PAC in M1 during walking predicted freezing severity and cognitive burdens exacerbate freezing through a "resources-competition" way. STN-DBS alleviated FOG by both reducing cortical PAC and increasing cortical resilience to excessive PAC. Based on these findings, we proposed the novel "bandwidth model," which extends the current multi-circuit hypothesis of FOG and may aid the development of next-generation neuromodulation therapy for FOG.

Materials and methods

Subject identification

Patients with Parkinson's disease who were scheduled to undergo DBS surgery at Beijing Tiantan Hospital were recruited prospectively from October 2019 to April 2021. Inclusion criteria included: 1) diagnosis of idiopathic Parkinson's disease according to the UK brain bank criteria; 2) clinical FOGs can be successfully induced as confirmed by at least one experienced movement disorders neurologist; 3) FOG reached moderate severity as attested by Freezing of Gait Questionnaire score over 10; and (4) aged between 50 and 80 years. Patients were excluded if they 1) were unable to walk independently in the OFF-medication condition; 2) demonstrated severe cognitive impairment making cooperation impossible; and (3) had prominent tremors (any item of the MDS-UPDRS 3.15–3.18 ≥3). Overall, 16 patients were included in this study. This study was in agreement with the Declaration of Helsinki, approved by the IRB of Beijing Tiantan Hospital (KY 2018-008-01), registered in the Chinese Clinical Trial Registry (ChiCTR1900026601), and conducted under the supervision of an authoritative third party (China National Clinical Research Center for Neurological Diseases). All patients signed written informed consent.

DBS and electrocorticography strip electrode implantation

DBS electrodes were placed in the bilateral STN as previously reported[19]. Briefly, DBS electrodes (model L301, Pins Medical, China) were implanted into the T2-weighted MRI identified STN target using a Leksell stereotactic system (Elekta Instrument AB, Stockholm, Sweden) under local anesthesia. Intraoperative microelectrode recording measuring the length of the DBS trajectory in the STN and macro-stimulation tests were conducted for trajectory selection. A CT scan was performed to confirm the location of the lead and to look for any signs of cerebral hemorrhage after surgery.

The subdural ECoG strip (HKHS, Beijing, China), composed of eight stainless steel contacts of 4 mm total diameter, 2.5 mm exposed diameter, and 10 mm spacing interval (except one subject was implanted with the 30 contact strip electrodes with 3 mm total diameter, 1.7 mm exposed diameter and 5 mm spacing), was placed in the right M1 region through the same burr hole as the DBS electrodes. Preoperative high-resolution computer tomography (CT) with the stereotactic frame markers attached was computationally fused to the anatomical T1-weighted MRI, enabling stereotactic planning and confirmation that the distance between the burr hole and the M1 is within the range of the ECoG strip length. After surgery, the position of the ECoG strip was confirmed with a CT scan and 3D cortical surface reconstruction[20]. The exemplary postoperative CT-MRI fused image and the surface reconstruction showing the position of the ECoG and DBS electrodes are displayed in **Fig. 1A, B**. ECoG strips were taken out at the second stage of DBS surgery when the pulse generator connected to DBS electrodes was implanted. The average duration of lead externalization was 8.9 ± 2.3 days. No incision infections or other hardware-related complications were observed in the perioperative period in any of the included patients.

Experimental protocol and motion capture system

Patients started to complete experimental tasks in the gait laboratory 3–5 days after electrode implantation. All antiparkinsonian medication was stopped at least 12 hours, and stimulation was stopped 2 hours before all recordings. Motor tasks were conducted under three conditions; no-stimulation, high-frequency stimulation (HFS, 130 Hz), and low-frequency stimulation (LFS, 60 Hz). The no-stimulation condition was always tested first, with the order of HFS and LFS being randomly counterbalanced across patients (HFS first in 9 patients, LFS first in 7 patients). A 30–60 minutes wash-in period was set to prepare patients for the

upcoming tasks conducted in stimulation conditions. All subjects were blinded to their stimulation parameters during the experiment. We used a portable analog stimulator (T901, Pins Medical, Beijing, China) to deliver square biphasic pulses in a bipolar configuration. Stimulation bandwidth was always set to 60 μs. Stimulation voltage was optimized according to the patient's feedback on motor improvement and the results of simplified motor test batteries.

Standard experimental tasks started with a 3-min of rest sitting and a 3-min of rest standing recording. During rest sitting & standing, patients were asked to keep relaxed and look at the cross sign hanging on the wall approximately 2 meters away. After that, patients were equipped with 22 sensors in both lower limbs (one in the foot, one in the heel, four in the shank, four in the thigh, and one in the waist, both sides), and completed a 5-meter back-and-forth (10 meters in total) timed up-and-go task (**Fig. 1C**). All walkings were captured using an optoelectronic system (CODA, Charnwood Dynamics Ltd, UK), which computed the 3D coordinates of the 22 lower limb sensors in real-time with a sampling rate of 100 or 200 Hz. Each back-and-forth walking was counted as one walking trial. In each stimulation condition, patients completed at least four trials of normal walking. As opposed to the "normal walking," patients also completed at least four trials of "dual-tasking walking," during which patients were asked to perform extra cognitive tasks while walking. Cognitive tasks were randomly assigned, including calculation, listing animal names, and transferring coins between hands. The whole course of the motor experiment was completed OFF-medication and was video recorded using a wide-angle camera synchronized with motion tracking.

Determination and quantification of freezing

Two independent raters clinically assessed all walking trials by examining the raw video recordings and the optoelectronics-based lower limb motion track replays. The two raters each gave judgments on whether a trial contained freezing and when the freezing occurred. We also adopted a freezing index (FI) approach to objectively determine and quantify freezings[21], and deposited the code for computing FI from 3D optoelectronics data on https://github.com/zixiao-yin/ecogFog. Briefly, we first transformed the coordinate data recorded by the optoelectronic sensors to acceleration data by calculating differencing twice (Python function *diff*). Spectrum analysis was then performed on the transformed acceleration data with respect to the forward walking direction using the fast Fourier transform[13]. The FI was computed as the ratio of power between the "freezing band" (3-8 Hz) and the

"locomotion band" (0–3 Hz)[21] in a 6s-sliding window centered in *t* with a step size of 0.1 s. The final FI was the average of eight sensor channels that were least contaminated (four on each side, including foot, shank, thigh, and waist). A "freezing threshold" was set to "3"[21]. Notably, because FI is a dynamic measurement, we defined that if FI dropped from above "3" to a value between "2" and "3" and then rose back to above "3", this was considered as one continuous freezing event rather than two. But if the FI dropped from above "3" to a value lower than "2", this marked the end of the freezing. Setting "2" as a "lower freezing threshold" was based on evidence that the lowest individual freezing threshold is around "2"[22]. The period lasting from the first to the last time point where FI is above "3" in a freezing event was referred to as the duration of a freezing event (**Fig. 1D**). In each trial, the number of freezing and the duration of each freezing event were counted and calculated. In addition, we classified each walking trial as a freezing trial or a nonfreezing trial based on whether it contained a freezing event. Only trials with consistent judgments between subjective and objective assessments were qualified for further analysis. Inconsistent trials were excluded, as their uncertainty may contaminate both the freezing and nonfreezing groups.

Potential recordings and contact selection

The JE-212 amplifier (Nihon Kohden, Tokyo, Japan) was used to record common average ECoG potentials. A cup Ag/AgCl electroencephalogram electrode placed on the subject's forehead was set as the ground. Signals were recorded at a sampling rate of 2,000 Hz, bandpass filtered at 0.08 and 600 Hz, and amplified ×195. We used a DC channel to synchronize ECoG potentials and the optoelectronic motion capture system. In the offline analysis, the ECoG potentials of each contact were re-referenced to its closest contact, resulting in seven bipolar cortical channels. We used a notch filter (Butterworth filter, bandwidth = 4 Hz, order = 3) to reject the ambient noise of 50 Hz and harmonics and the stimulation artifact of 60/130 Hz and harmonics. Signals were downsampled to 1,000 Hz for further analysis. Out of the seven bipolar channels, the channel selected for analysis was constituted by the contact pair where at least one of the contacts was landed on M1. This could be the premotor-M1, the M1-M1, or the M1-S1 contact pairs, depending on which pair demonstrated the highest PAC during rest siting[17]. The coordinates of the selected contact pairs covering M1 for each subject are shown in **Supplementary Table 1**. In addition, the

S1-post S1 contact pair was selected as a control channel, which represented signals that were irrelevant to the motor cortex.

Power spectral density calculation

We employed the Welch periodogram method (Python MNE function *psd_welch*[23]) to calculate power spectral density (PSD) using a fast Fourier transform of 512 points. This rendered a frequency resolution of 1.95 Hz. And a 50% overlap using a Hanning window was employed to reduce edge effects. PSD was transformed into the log scale. In the computation of the beta (13-30 Hz) and gamma (50–200 Hz) power, a further inner-subject normalization was made by calculating the percentage of the total power in each subject.

Phase-amplitude coupling analysis

Phase-amplitude coupling was calculated using a method that has been previously described[24]. Briefly, potentials recorded in ECoG were first bandpass filtered into a low frequency band (6-50 Hz in a 2-Hz step, without overlap) and a high frequency band (50–200 Hz in a 4-Hz step, without overlap) using a 2-way zero phase lag finite impulse response filter. Then, the instantaneous phase of the low frequency bandpass filtered signal and the instantaneous amplitude of the high frequency filtered signal were extracted through the Hilbert transform. The modulation index (MI) was derived using the Kullback-Leibler distance that measures the divergence between the probability distribution of high-frequency amplitudes and uniform distribution. The obtained MI was normalized by calculating the z-score of 200 surrogates generated by randomly swapping amplitudes time blocks[25]. Z-scored PAC computed for multiple frequencies of phase and amplitude can be demonstrated as a comodulogram (**Fig. 2A**). We used the Tensorpac toolbox (https://etiennecmb.github.io/tensorpac/)[26] to conduct all PAC calculations.

Trial analysis

For data recorded during rest sitting and standing, the first continuous 30 s data without artifact and movement were selected for analysis. For data recorded during walking, the whole length of data recorded in completing the walking trial was analyzed. PAC was calculated using a 10 s sliding window with a 5 s step size and averaged among windows. A 10 s sliding window was selected because the shortest walking trial lasted 11 s. Ten-second is a reliable calculation length, which contains over 130 cycles of beta-band phase[27].

Supplementary Fig. 1A, B show that the 10s-window MIs were highly linearly correlated with the 30s-window MIs in both the trial wise correlation (Spearman r = 0.88, $P < 0.001$) and the subject wise correlation (Spearman r = 0.97, $P < 0.001$). PAC statistics were then compared among the standing, freezing, and nonfreezing trials.

Episode analysis

It should be noted that in freezing trials, it was not the case that at all time points the subject was under freezing. Instead, a freezing trial contained both the episodes where the subject was freezing and episodes where the subject was walking stably. Thus, in each freezing trial, we extracted a continuous 5 s nonfreezing-episode with the lowest average FI and termed it as the freezing trials' nonfreezing episode (FN), which best represented a period of clear, rhythmic walking in a freezing trial. Besides, the freezing episode, where FI exceeded three, in a freezing trial was extracted and termed as the freezing trials' freezing episode (FF). For nonfreezing trials, a continuous 5 s episode with the lowest average FI was also extracted and termed as the nonfreezing trials' normal walking episode (NN), served as a control. The schematic diagram of the episode extraction is shown in **Fig. 3A, B**. Episodes with the same type extracted from trials in the same stimulation condition were concatenated for each subject. A 10 s sliding window with a 1 s step size was employed for PAC computation to improve data utilization. In the comparison of PAC between the three types of episodes, an inner-subject normalization was made by calculating the percentage relative change with respect to NN and scaling to the max value:

$$\text{percentage relative change}^{k} = \frac{PAC^{k} - PAC^{NN}}{max(abs(PAC^{k,NN}))} \times 100\%$$

Where "*abs*" represents the absolute value, with k = {FN, FF}.

Analysis on dual-tasking and stimulation

Freezing severity and PAC statistics were compared between dual-task and no-task conditions, and stimulation and no-stimulation conditions. Condition-wise freezing severity was measured using three indices: (1) freezing time proportion, referred to as the proportion of the total duration of freezing to the total time spent on walking; (2) freezing frequency per trial, calculated by dividing the total count of freezing by the total count of trials performed; and (3) duration per freezing, calculated by dividing the total duration of freezing by the total

count of freezing. Condition-wise PAC was calculated by averaging PAC in trials that were performed under the same condition. In analyzing the effect of stimulation, we further correlated the stimulation-induced improvement of freeing severity to the stimulation-induced reduction of PAC. The improvement/reduction was normalized by calculating percentage change with respect to the no-stimulation condition for each subject:

$$\text{percentage change} = \frac{value^{NS} - value^{STIM}}{abs(value^{NS})} \times 100\%$$

Where "*value*" represents the three indices of freezing severity and PAC, "*abs*" represents the absolute value, "*NS*" represents the no-stimulation condition, and "*STIM*" represents the stimulation condition.

Statistical analysis

Statistical analyses were performed using nonparametric tests whenever possible (signed-rank tests, Kruskal-Wallis test, Friedman test, and Spearman's correlation) because of the non-normal distribution of most studied variables. Linear mixed effect (LME) model was used for repeated measures data where the subject was a random effect, and a random intercept was utilized. A 2-tailed P-value < 0.05 was considered significant, with multiple comparisons corrected using the Bonferroni correction. All statistical analyses were performed using Python 3.

Data availability

All relevant codes reported in the paper can be freely accessed without restriction. The raw data that support the findings of this study are available from the corresponding author upon reasonable request after approval of local IRB.

Results

Overall, 16 patients were included in this study and were implanted with the ECoG and DBS electrodes (see **Figure 1A, B** for exemplar electrode locations of sub5). **Table 1** summarizes the demographics, outcomes of motor assessments, and stimulation parameters used during lead externalization. The 16 subjects were on average 66.1 years old, with an average disease duration of 9.3 years. The average preoperative MDS-UPDRS III scored 50.1 in the OFF-

medication state, which was reduced to 25.1 in the ON-stimulation/OFF-medication state, rendering an average motor improvement of 49.9%. Two subjects were excluded from later analyses: sub7 was unable to complete the required number of walking trials due to severe gait problems, and sub10's subdural electrode was shifted, not covering M1. Thus, the electrophysiology and motion data from the remaining 14 subjects were analyzed. A total of 451 walking trials at a self-selected pace were completed by the 14 patients (**Fig. 1C**). After independent subjective and objective inspections, consensus between the two approaches was reached in 407 trials on whether the trial contained freezing (inter-rater reliability = 90.2%). Among the 407 trials, 114 were freezing trials with an average trial duration of 85.9 s, including 294 freezing events with average event duration of 11.5 s and a total freezing duration of 3,384 s, and 293 were nonfreezing trials, with an average trial duration of 24.1 s and a total walking duration of 7,073 s. All recordings were conducted in the OFF-medication state.

Freezing trials had higher PAC in M1, which was not induced by dual-tasking or velocity change

The comodulograms of group-level PAC during rest standing, freezing, and nonfreezing trials were shown in **Fig. 2A**. We observed the highest PAC during rest standing ($P_{Bonferroni}$ for standing *vs*. nonfreezing < 0.001, for standing *vs.* freezing = 0.042; signed-rank test, **Fig. 2B**), and a significantly higher PAC during freezing trials than during nonfreezing trials in the M1 (P = 0.013, signed-rank test, **Fig. 2B**), but not the postcentral gyrus area (P = 0.375, signed-rank test, **Supplementary Fig. 2A-C**). Consistent results were also revealed when PAC was computed using a 30 s window (**Supplementary Fig. 1C**). Taking sub8 as an example, the preferred phases of coupling were similar, but the intensities of coupling went down from standing to freezing and nonfreezing trials (**Fig. 2C**). Notably, we did not observe significant differences in cortical beta and gamma power between freezing and nonfreezing trials, while higher beta power (P = 0.007, signed-rank test) and lower gamma power (P = 0.016, signed-rank test) were indeed observed during the rest standings compared to that during walking (**Supplementary Fig. 3A, B**).

Given that dual tasks (e.g., calculation while walking) have been conducted in a number of trials to induce freezing, we asked if the higher PAC during freezing trials could be directly related to dual tasks rather than freezing. We first validated that dual-task trials did have

higher freezing severity than no-task trials (P = 0.041 for freezing time proportion, P = 0.009 for freezing frequency, signed-rank test, **Fig. 2D**). But interestingly, dual-task trials had similar PAC levels to no-task trials (P = 0.278, signed-rank test, **Fig. 2E**), and dual tasking itself was not correlated with high PAC level (Spearman r = 0.030, P = 0.583). If we controlled the factor of freezing by analyzing only the nonfreezing trials, we found that dual-task nonfreezing trials had even significantly lower PAC than no-task trials (P = 0.006, signed-rank test, **Fig. 2F**). These results indicated that PAC and dual tasking were not directly associated, but may interact in a more complex way.

Given that PAC in M1 can be related to bradykinesia in Parkinson's disease[15], we assessed if higher PAC during freezing trials could be induced by the reduced walking velocity per se rather than freezing. We instructed five subjects to complete extra trials of intentionally fast- and slow-velocity walking, and controlled the factor of freezing by analyzing nonfreezing trials only (n = 72). We found that the average speed (total distance/total time) was significantly different among fast-, normal- and slow-speed trials (tested through LME models, **Supplementary Fig. 4A**), while no difference was observed in PAC (**Supplementary Fig. 4B, C**). This suggested that PAC was not directly associated with walking velocity, and the higher PAC observed in freezing trials was unlikely to be induced by velocity change.

Nonfreezing episodes in freezing trials also had higher PAC, which predicted freezing severity

There are two explanations for the observed high PAC in freezing trials. First, PAC peaked only when freezing occurred while maintaining a normal level during nonfreezing walking. Second, PAC was constantly at an abnormally higher level during freezing trials, not limited to the period where freezing occurred. To investigate, we compared PAC levels between different walking episodes (**Fig. 3A, B**). We found that PACs of the FN and FF were in similar levels (P = 0.147, signed-rank test), while both were significantly higher than that of the NN (P = 0.003 for FN, P = 0.007 for FF, signed-rank test, **Fig. 3C**). This trend was evident in almost each subject (**Fig. 3D**) and also held true after correcting the different FI level using LME model (FN *vs.* NN: β = 0.427, 95% CI = 0.104 to 0.749, P = 0.010; FF *vs.* NN: β = 0.615, 95% CI = 0.060 to 1.170, P = 0.030). These results indicated the nonfreezing walking episodes in freezing trials were also electrophysiologically abnormal.

To investigate how different walking episodes were related to clinical freezings, we correlated the PAC in episodes of rest standing (PAC_{stand}), stable walking (FN and NN, PAC_{stable}), and unstable walking (FF, and 5 s with highest FI in the nonfreezing trial, $PAC_{unstable,}$ **Fig. 4A**) to the three indices of freezing severity after regressing out the effect of subjects using LME models. We observed that PAC_{stable}, but not $PAC_{unstable,}$ were significantly correlated with all three indices of freezing severity (Bonferroni corrected $P < 0.05$, **Fig. 4B-D)**.

The influence of DBS on PAC and freezing

We next explored how STN-DBS may act on M1 PAC and freezing severity. Given that we did not observe significant differences between HFS and LFS conditions in any of the trial-PAC, episode-PAC, and freezing severity (although a trend favoring LFS manifested as lower trial PAC and less freezing were observed, **Supplementary Fig. 5A-C**), HFS and LFS are collectively referred to as STIM in further analysis. We found that stimulation significantly reduced the three types of PAC and simultaneously alleviated freezing severity measured through the three aforementioned indices **(Fig. 5A, B)**. When we further correlated the STIM-induced PAC reduction to the STIM-induced percentage improvement of freezing severity, only PAC_{stable} remained significant in all three indices of freezing measurements (Bonferroni corrected $P < 0.05$, **Fig. 5C-E**). These results suggested that STN-DBS improved FOG by reducing PAC during stable walking.

It's also interesting to note, even in STIM trials that were at a similar PAC level to no-stimulation trials (by picking out PAC-matched trials with z-scored PAC between 0-0.4, $P = 0.455$, signed-rank test, **Fig. 6A, B**), clinical freezing was still significantly improved in these STIM trails as compared to no-stimulation trials (**Fig. 6C-E**). These results suggested that the freezing alleviation induced by STN-DBS was not due solely to the PAC reduction. Other modulation ways may also be in play here, such as elevating cortical resistance to excessive PAC.

The "bandwidth model" of FOG

Finally, based on the above findings, we formalized a theoretical "bandwidth model" of FOG to organically explain these observations (**Fig. 7**). The "bandwidth" mimics the processing resource in human brains. The model consists of three main elements, (I) the baseline

occupation, (II) the dynamic fluctuation, and (III) the bandwidth limit. The "baseline occupation" depicts the occupation of cortical processing resources by the elevated neuronal synchrony, which can be quantified through M1 PAC and reflects the degree of motor impairment under a certain condition. The "dynamic fluctuation" reflects the instantaneous cognitive burden, which changes dynamically with time. And the "bandwidth limit" defines a threshold when it is exceeded, information processing overloads and freezing occurs. The blank zone laid between the bandwidth limit and baseline occupation is the "available bandwidth," whose area represents the instant available neural processing resource. STN-DBS exerts therapeutic effects on FOG by both reducing the baseline occupation and elevating the bandwidth limit.

Discussion

In this study, leveraging direct motor cortex recording, 3D-motion tracking, and walking task trials, we demonstrate that (I) freezing trials had higher PAC in M1, and the high PAC was not induced by dual-tasking or velocity change; (II) nonfreezing episodes in freezing trials also had excessive PAC, which predicted freezing severity; and (III) STN-DBS reduced PAC and alleviated clinical freezing, while the PAC reduction was not the only cause of freezing alleviation. A "bandwidth model" was further proposed to explain the occurrence and treatment of FOG.

We linked our observations to the model as follows. (I) *Observed phenomenon:* M1 PAC was significantly and constantly higher in freezing trials than in nonfreezing trials (**Fig. 2, 3**) and was correlated with freezing severity during stable walking (**Fig. 4**). *Reflected in the model:* M1 PAC was indicative of the baseline occupation. When holding the dynamic fluctuation and bandwidth limit on, the higher the baseline occupation was, the higher the chance freezings were to occur. (II) *Observed phenomenon:* freezings were more likely to occur during dual-task trials, which, however, were not associated with high PAC. Contrarily, if picking only the nonfreezing trials, dual-tasks were accompanied with a lower PAC (**Fig. 2 D-F**). *Reflected in the model:* a higher chance of freezing in dual-task trials was the result of the elevated dynamic fluctuation rather than the baseline occupation. While due to the larger fluctuation, only trials with low baseline occupation could avoid exceeding bandwidth limit, resulting in the observed low PAC in nonfreezing dual-task trials. (III) *Observed phenomenon:* stimulation significantly reduced PAC while simultaneously improving

freezing. The STIM-induced reduction of PAC was correlated with the STIM-induced improvement of freezing (**Fig. 5**). *Reflected in the model:* stimulation reduced baseline occupation, and whose reduction should be in accordance with the lowering of freezing probability when the dynamic fluctuation and bandwidth limit were kept generally constant. (IV) *Observed phenomenon:* STIM trials had lower freezing severity than NS trials even when under similar levels of PAC (**Fig. 6**). *Reflected in the model:* except for reducing baseline occupation, DBS improved FOG also through enhancing bandwidth limit.

To our knowledge, four classical models have been proposed hypothesizing the mechanisms of FOG[28]. (I) The "threshold model"[29] indicates that the motor deficits such as reduced stride amplitude and asymmetrical step sizes could accumulate during walking. When accumulated motor abnormality reaches a threshold, FOG occurs. (II) The "cognitive model"[30] holds that FOG is triggered by impaired conflict resolution and is exacerbated by freezing-related executive dysfunction. One evidence is that freezers could have higher variability than non-freezers in selecting swing limb when initiating gait[31]. (III) The "decoupling model"[32] stresses that the decoupling between perceived movement intention and the actual release of gait initiation results in FOG. This explains why patients describe freezing as having "their feet glued to the ground." (IV) The "interference model"[33] explains the occurrence of FOG as the breakdown of parallel information processing of motor, cognitive and limbic circuits. Increasing the number or the difficulty of concurrent tasks could induce FOG. Notably, most models focused on a feature of freezing and explained changes in other features as secondary. By comparison, the "interference model" gave a more comprehensive picture stressing the joint participation of motor, cognitive, and limbic circuits in FOG, which was further supported by later studies[34–36].

One novel aspect of our model is that it provides an approach, i.e., PAC in M1, to quantitatively track dynamic changes of the motor circuit in the occurrence of FOG. Previously, abnormal PAC has been documented in the M1 area in both animal models and humans with Parkinson's disease. It was shown that beta-gamma PAC is correlated with the severity of bradykinesia and decreases during movement[17,37,38]. In our study, we also observed reduced PAC during walking as compared to standing. We hypothesize that the release of cortical broad-gamma amplitude from low oscillation phases may facilitate the motor execution[39]. While by demonstrating that trials with significantly different walking velocities had similar PAC as long as freezing was not occurred (**Supplementary Fig. 3**), we showed that PAC was not a mere reflection of movement intensity but did indicate motor

impairments related to FOG. PAC as one class of cross-frequency-coupling is considered a vital fundamental mechanism underlying information processing[16]. In normal states, the modulation of the high-frequency amplitude by the low-frequency rhythms is highly dynamic and task-specific[17,40]. In the pathological PD OFF state, perpetually elevated M1 PAC may reflect a restricted cortical activation state in which M1 neurons are not able to respond dynamically to communication across other cortical and subcortical circuits. Given that M1 is a crucial node in human gait physiology[10], a pathological hypersynchrony in M1, through entrainment and phase locking of the broad-gamma activity to the beta carrier rhythm, could underpin the pathological basis for FOG in PD. Alternatively, elevated PAC may reflect changes in the sharpness and asymmetry of cortical beta band waves, representing the excessive neural synchrony in the basal ganglia-thalamocortical loop[41,42]. Here, our data reveal moderate correlations of PAC and beta waveform shape and sharpness asymmetry measures (**Supplementary Figure 6).** This suggests, neither mechanism alone can explain PAC in our study and that either one demonstrates a form of excessive synchrony in M1 and could be relevant to the pathology of FOG.

On the other hand, the quantification of motor circuit abnormality makes it possible to further investigate how specifically motor dysfunction interacts with cognitive burdens during freezing, therefore extending the classical "interference model" of FOG. By showing that dual tasking did not directly impact the strength of PAC in M1, while only trials with low PAC could resist freezing when performing extra concurrent tasks, we reveal that motor and cognitive processing are actually competing for finite computational capacity. Both walking and dual tasking require cortical processing resources, while the elevation of PAC due to the parkinsonian state makes walking take more resources. This leads to a corresponding decrease of available resources for cognitive processing, increases the probability of "information overload," and ultimately causes FOG.

Our model also explains how STN-DBS may act on the pathology of FOG. Previous reports focused more on the direct improvement on motor function, suggesting that STN-DBS may exert its effect on freezing through improving overall gait speed, stride length, trunk flexion, or anticipatory postural adjustments[43–46]. Our model integrates motor improvement into a larger explanatory framework. Loss of dopamine can lead to changes in local and distant neural population activity[47,48]. DBS can disrupt abnormal information flow in basal ganglia circuits, potentially by dissociating input and output signals of the STN[49,50]. This may result in the restoration of a normalized cortical activity pattern. Besides, the antidromic activation

of the cortico-STN fibers through DBS may desynchronize cortical neurons[51,52] and increase their ability to transfer information individually, leading to higher information-coding capacity[53,54]. These effects, presented as the improved motor function and the lower cortical PAC (analogs to lower baseline occupation), contribute to enlarged disposable computational capacity (analogs to higher available bandwidth) that can be used to deal with dynamic cognitive burdens and therefore reduces freezing probability. Notably, since the STN is also actively involved in cognitive processings[55], investigating whether STN-DBS eases freezing also through modulating cognitive circuit (i.e., the dynamic fluctuation in our model) is warranted in the future.

Besides, our results provide evidence supporting the clinical utility of M1 PAC as a reliable feedback biomarker in the development of symptom-specific adaptive DBS. In previous reports, cortical PAC in human was almost exclusively recorded though ECoG in intraoperative settings[17,56,57] or through high-density scalp EEG[58,59]. While in both scenarios, a considerable extent of fixation/stationary is needed. It is understudied how PAC responds to and whether PAC can be measured during naturalistic movement[60]. Our data demonstrate that although general movement (i.e., walking) significantly reduced PAC compared to resting, the reduced PAC still indicates pathological conditions and responses to therapeutic DBS. Notably, results obtained in this study were based on PAC calculated in a 10 s window. In developing adaptive DBS, this slower control strategy, as opposed to the fast time scale burst-detecting strategy[61,62], may better track motor fluctuations over a period of time[63]. The latest Summit RC+S (Medtronic) study[64] employed a feedback time scale of 2-10 min in chronic at-home recordings. Longer data segment increases the signal-to-noise ratio helping better differentiate pathological from the physiological state, which may also be applied to PAC indices (e.g., PAC computed in 30 s window is approximately three times the PAC computed in 10 s window, **supplementary Fig. 1**). Overall, this study provides a neurophysiology approach to quantify the severity of motor abnormality in FOG. But notably, PAC in M1 cannot model the dynamic change of cognitive burden, which also plays a vital role in the occurrence of FOG. In fact, as per our model, it is the dynamic fluctuation, but not baseline occupation decides the exact time point freezing occurs when keeping bandwidth limit constant. Therefore, future studies tracking changes in the cognitive/limbic circuit during freezing, e.g., through recording heart rate change[65], or neural activities from the prefrontal cortex[34], would immensely enrich the proposed model.

In conclusion, this study highlighted the key role of M1-PAC in the occurrence and treatment of FOG. Based on this, the proposed "bandwidth model" adequately explains the multi-circuit pathology of FOG, uncovers the potential mechanism by which STN-DBS alleviates FOG, and may foster next-generation neuromodulation therapies targeting gait freezing in parkinsonian patients.

Acknowledgements

We would like to present our acknowledgments to our patients for participating in this project, to Dr. Zeyu Wang for her assistance on the art designing of the illustrations, to Dr. Qiang Wang for his critical review.

Funding

This study was funded by the National Natural Science Foundation of China (81830033, 61761166004, 81870888) and the Capital Medical Development Research Fund (2018-2Z-1076).

Competing interests

The authors declare no competing financial interests.

Supplementary material

Supplementary material is available at *Brain* online.

References

1. Nutt JG, Bloem BR, Giladi N, Hallett M, Horak FB, Nieuwboer A. Freezing of gait: moving forward on a mysterious clinical phenomenon. *Lancet Neurol*. 2011;10(8):734-744. doi:10.1016/S1474-4422(11)70143-0

2. Moore O, Peretz C, Giladi N. Freezing of gait affects quality of life of peoples with Parkinson's disease beyond its relationships with mobility and gait. *Mov Disord*. 2007;22(15):2192-2195. doi:10.1002/mds.21659

3. Muslimovic D, Post B, Speelman JD, Schmand B, de Haan RJ, CARPA Study Group. Determinants of disability and quality of life in mild to moderate Parkinson disease. *Neurology*. 2008;70(23):2241-2247. doi:10.1212/01.wnl.0000313835.33830.80

4. Fasano A, Daniele A, Albanese A. Treatment of motor and non-motor features of Parkinson's disease with deep brain stimulation. *Lancet Neurol*. 2012;11(5):429-442. doi:10.1016/S1474-4422(12)70049-2

5. Bohnen NI, Costa RM, Dauer WT, et al. Discussion of Research Priorities for Gait Disorders in Parkinson's Disease. *Mov Disord*. Published online December 22, 2021. doi:10.1002/mds.28883

6. Thevathasan W, Cole MH, Graepel CL, et al. A spatiotemporal analysis of gait freezing and the impact of pedunculopontine nucleus stimulation. *Brain*. 2012;135(Pt 5):1446-1454. doi:10.1093/brain/aws039

7. Xie T, Bloom L, Padmanaban M, et al. Long-term effect of low frequency stimulation of STN on dysphagia, freezing of gait and other motor symptoms in PD. *J Neurol Neurosurg Psychiatry*. 2018;89(9):989-994. doi:10.1136/jnnp-2018-318060

8. Mei S, Li J, Middlebrooks EH, et al. New Onset On-Medication Freezing of Gait After STN-DBS in Parkinson's Disease. *Front Neurol*. 2019;10:659. doi:10.3389/fneur.2019.00659

9. Annweiler C, Beauchet O, Bartha R, et al. Motor cortex and gait in mild cognitive impairment: a magnetic resonance spectroscopy and volumetric imaging study. *Brain*. 2013;136(3):859-871. doi:10.1093/brain/aws373

10. McCrimmon CM, Wang PT, Heydari P, et al. Electrocorticographic Encoding of Human Gait in the Leg Primary Motor Cortex. *Cereb Cortex*. 2018;28(8):2752-2762. doi:10.1093/cercor/bhx155

11. Jha M, Jhunjhunwala K, Sankara BB, et al. Neuropsychological and imaging profile of patients with Parkinson's disease and freezing of gait. *Parkinsonism Relat Disord*. 2015;21(10):1184-1190. doi:10.1016/j.parkreldis.2015.08.009

12. Shine JM, Matar E, Ward PB, et al. Exploring the cortical and subcortical functional magnetic resonance imaging changes associated with freezing in Parkinson's disease. *Brain*. 2013;136(Pt 4):1204-1215. doi:10.1093/brain/awt049

13. Pozzi NG, Canessa A, Palmisano C, et al. Freezing of gait in Parkinson's disease reflects a sudden derangement of locomotor network dynamics. *Brain*. 2019;142(7):2037-2050. doi:10.1093/brain/awz141

14. Petrucci MN, Neuville RS, Afzal MF, et al. Neural closed-loop deep brain stimulation for freezing of gait. *Brain Stimul*. 2020;13(5):1320-1322. doi:10.1016/j.brs.2020.06.018

15. de Hemptinne C, Swann NC, Ostrem JL, et al. Therapeutic deep brain stimulation reduces cortical phase-amplitude coupling in Parkinson's disease. *Nat Neurosci*. 2015;18(5):779-786. doi:10.1038/nn.3997

16. Canolty RT, Knight RT. The functional role of cross-frequency coupling. *Trends Cogn Sci*. 2010;14(11):506-515. doi:10.1016/j.tics.2010.09.001

17. de Hemptinne C, Ryapolova-Webb ES, Air EL, et al. Exaggerated phase-amplitude coupling in the primary motor cortex in Parkinson disease. *Proc Natl Acad Sci U S A*. 2013;110(12):4780-4785. doi:10.1073/pnas.1214546110

18. Lewis SJG, Shine JM. The Next Step: A Common Neural Mechanism for Freezing of Gait. *Neuroscientist*. 2016;22(1):72-82. doi:10.1177/1073858414559101

19. Yin Z, Bai Y, Zou L, et al. Balance response to levodopa predicts balance improvement after bilateral subthalamic nucleus deep brain stimulation in Parkinson's disease. *NPJ Parkinsons Dis*. 2021;7(1):47. doi:10.1038/s41531-021-00192-9

20. Hamilton LS, Chang DL, Lee MB, Chang EF. Semi-automated Anatomical Labeling and Inter-subject Warping of High-Density Intracranial Recording Electrodes in Electrocorticography. *Front Neuroinform*. 2017;11:62. doi:10.3389/fninf.2017.00062

21. Moore ST, Yungher DA, Morris TR, et al. Autonomous identification of freezing of gait in Parkinson's disease from lower-body segmental accelerometry. *J Neuroeng Rehabil*. 2013;10:19. doi:10.1186/1743-0003-10-19

22. Moore ST, MacDougall HG, Ondo WG. Ambulatory monitoring of freezing of gait in Parkinson's disease. *J Neurosci Methods*. 2008;167(2):340-348. doi:10.1016/j.jneumeth.2007.08.023

23. Gramfort A, Luessi M, Larson E, et al. MEG and EEG data analysis with MNE-Python. *Front Neurosci*. 2013;7:267. doi:10.3389/fnins.2013.00267

24. Tort ABL, Kramer MA, Thorn C, et al. Dynamic cross-frequency couplings of local field potential oscillations in rat striatum and hippocampus during performance of a T-maze task. *Proc Natl Acad Sci U S A*. 2008;105(51):20517-20522. doi:10.1073/pnas.0810524105

25. Bahramisharif A, van Gerven MAJ, Aarnoutse EJ, et al. Propagating neocortical gamma bursts are coordinated by traveling alpha waves. *J Neurosci*. 2013;33(48):18849-18854. doi:10.1523/JNEUROSCI.2455-13.2013

26. Combrisson E, Nest T, Brovelli A, et al. Tensorpac: An open-source Python toolbox for tensor-based phase-amplitude coupling measurement in electrophysiological brain signals. *PLoS Comput Biol*. 2020;16(10):e1008302. doi:10.1371/journal.pcbi.1008302

27. Jurkiewicz GJ, Hunt MJ, Żygierewicz J. Addressing pitfalls in phase-amplitude coupling analysis with an extended modulation index toolbox. *Neuroinformatics*. 2021;19(2):319-345. doi:10.1007/s12021-020-09487-3

28. Nieuwboer A, Giladi N. Characterizing freezing of gait in Parkinson's disease: models of an episodic phenomenon. *Mov Disord*. 2013;28(11):1509-1519. doi:10.1002/mds.25683

29. Plotnik M, Giladi N, Hausdorff JM. Is freezing of gait in Parkinson's disease a result of multiple gait impairments? Implications for treatment. *Parkinsons Dis*. 2012;2012:459321. doi:10.1155/2012/459321

30. Vandenbossche J, Deroost N, Soetens E, et al. Freezing of gait in Parkinson's disease: disturbances in automaticity and control. *Front Hum Neurosci*. 2012;6:356. doi:10.3389/fnhum.2012.00356

31. Okada Y, Fukumoto T, Takatori K, Nagino K, Hiraoka K. Variable initial swing side and prolonged double limb support represent abnormalities of the first three steps of gait initiation in patients with Parkinson's disease with freezing of gait. *Front Neurol*. 2011;2:85. doi:10.3389/fneur.2011.00085

32. Jacobs JV, Nutt JG, Carlson-Kuhta P, Stephens M, Horak FB. Knee trembling during freezing of gait represents multiple anticipatory postural adjustments. *Exp Neurol*. 2009;215(2):334-341. doi:10.1016/j.expneurol.2008.10.019

33. Lewis SJG, Barker RA. A pathophysiological model of freezing of gait in Parkinson's disease. *Parkinsonism Relat Disord*. 2009;15(5):333-338. doi:10.1016/j.parkreldis.2008.08.006

34. Ehgoetz Martens KA, Hall JM, Georgiades MJ, et al. The functional network signature of heterogeneity in freezing of gait. *Brain*. 2018;141(4):1145-1160. doi:10.1093/brain/awy019

35. Lang S, Ismail Z, Kibreab M, Kathol I, Sarna J, Monchi O. Common and unique connectivity at the interface of motor, neuropsychiatric, and cognitive symptoms in Parkinson's disease: A commonality analysis. *Hum Brain Mapp*. 2020;41(13):3749-3764. doi:10.1002/hbm.25084

36. Herman T, Shema-Shiratzky S, Arie L, Giladi N, Hausdorff JM. Depressive symptoms may increase the risk of the future development of freezing of gait in patients with Parkinson's disease: Findings from a 5-year prospective study. *Parkinsonism Relat Disord*. 2019;60:98-104. doi:10.1016/j.parkreldis.2018.09.013

37. Devergnas A, Caiola M, Pittard D, Wichmann T. Cortical Phase-Amplitude Coupling in a Progressive Model of Parkinsonism in Nonhuman Primates. *Cereb Cortex*. 2019;29(1):167-177. doi:10.1093/cercor/bhx314

38. Malekmohammadi M, AuYong N, Ricks-Oddie J, Bordelon Y, Pouratian N. Pallidal deep brain stimulation modulates excessive cortical high β phase amplitude coupling in Parkinson disease. *Brain Stimul*. 2018;11(3):607-617. doi:10.1016/j.brs.2018.01.028

39. Yanagisawa T, Yamashita O, Hirata M, et al. Regulation of motor representation by phase-amplitude coupling in the sensorimotor cortex. *J Neurosci*. 2012;32(44):15467-15475. doi:10.1523/JNEUROSCI.2929-12.2012

40. Miller KJ, Hermes D, Honey CJ, et al. Human motor cortical activity is selectively phase-entrained on underlying rhythms. *PLoS Comput Biol*. 2012;8(9):e1002655. doi:10.1371/journal.pcbi.1002655

41. Cole SR, van der Meij R, Peterson EJ, de Hemptinne C, Starr PA, Voytek B. Nonsinusoidal beta oscillations reflect cortical pathophysiology in Parkinson's disease. *J Neurosci*. 2017;37(18):4830-4840. doi:10.1523/JNEUROSCI.2208-16.2017

42. Sherman MA, Lee S, Law R, et al. Neural mechanisms of transient neocortical beta rhythms: Converging evidence from humans, computational modeling, monkeys, and mice. *Proc Natl Acad Sci U S A*. 2016;113(33):E4885-4894. doi:10.1073/pnas.1604135113

43. Johnsen EL, Mogensen PH, Sunde NAa, Østergaard K. Improved asymmetry of gait in Parkinson's disease with DBS: Gait and postural instability in Parkinson's disease treated with bilateral deep brain stimulation in the subthalamic nucleus: Improved Asymmetry of Gait in PD with STN-DBS. *Mov Disord*. 2009;24(4):588-595. doi:10.1002/mds.22419

44. McNeely ME, Earhart GM. Medication and subthalamic nucleus deep brain stimulation similarly improve balance and complex gait in Parkinson disease. *Parkinsonism Relat Disord*. 2013;19(1):86-91. doi:10.1016/j.parkreldis.2012.07.013

45. Ferrarin M, Rizzone M, Lopiano L, Recalcati M, Pedotti A. Effects of subthalamic nucleus stimulation and L-dopa in trunk kinematics of patients with Parkinson's disease. *Gait Posture*. 2004;19(2):164-171. doi:10.1016/S0966-6362(03)00058-4

46. Bleuse S, Delval A, Blatt JL, Derambure P, Destée A, Defebvre L. Effect of bilateral subthalamic nucleus deep brain stimulation on postural adjustments during arm movement. *Clin Neurophysiol*. 2011;122(10):2032-2035. doi:10.1016/j.clinph.2011.02.034

47. McGregor MM, Nelson AB. Circuit Mechanisms of Parkinson's Disease. *Neuron*. 2019;101(6):1042-1056. doi:10.1016/j.neuron.2019.03.004

48. DeLong MR, Wichmann T. Circuits and circuit disorders of the basal ganglia. *Arch Neurol*. 2007;64(1):20-24. doi:10.1001/archneur.64.1.20

49. McIntyre CC, Grill WM, Sherman DL, Thakor NV. Cellular effects of deep brain stimulation: model-based analysis of activation and inhibition. *J Neurophysiol*. 2004;91(4):1457-1469. doi:10.1152/jn.00989.2003

50. Bucher D, Goaillard JM. Beyond faithful conduction: short-term dynamics, neuromodulation, and long-term regulation of spike propagation in the axon. *Prog Neurobiol*. 2011;94(4):307-346. doi:10.1016/j.pneurobio.2011.06.001

51. Li Q, Qian ZM, Arbuthnott GW, Ke Y, Yung WH. Cortical effects of deep brain stimulation: implications for pathogenesis and treatment of Parkinson disease. *JAMA Neurol*. 2014;71(1):100-103. doi:10.1001/jamaneurol.2013.4221

52. Chen W, de Hemptinne C, Miller AM, et al. Prefrontal-Subthalamic Hyperdirect Pathway Modulates Movement Inhibition in Humans. *Neuron*. 2020;106(4):579-588.e3. doi:10.1016/j.neuron.2020.02.012

53. Brittain JS, Brown P. Oscillations and the basal ganglia: motor control and beyond. *Neuroimage*. 2014;85 Pt 2:637-647. doi:10.1016/j.neuroimage.2013.05.084

54. Yin Z, Zhu G, Zhao B, et al. Local field potentials in Parkinson's disease: A frequency-based review. *Neurobiol Dis*. 2021;155:105372. doi:10.1016/j.nbd.2021.105372

55. Frank MJ, Samanta J, Moustafa AA, Sherman SJ. Hold your horses: impulsivity, deep brain stimulation, and medication in parkinsonism. *Science*. 2007;318(5854):1309-1312. doi:10.1126/science.1146157
56. Salimpour Y, Mills KA, Hwang BY, Anderson WS. Phase- targeted stimulation modulates phase-amplitude coupling in the motor cortex of the human brain. *Brain Stimul*. 2021;15(1):152-163. doi:10.1016/j.brs.2021.11.019
57. Kondylis ED, Randazzo MJ, Alhourani A, et al. Movement-related dynamics of cortical oscillations in Parkinson's disease and essential tremor. *Brain*. 2016;139(Pt 8):2211-2223. doi:10.1093/brain/aww144
58. Gong R, Wegscheider M, Mühlberg C, et al. Spatiotemporal features of β-γ phase-amplitude coupling in Parkinson's disease derived from scalp EEG. *Brain*. 2021;144(2):487-503. doi:10.1093/brain/awaa400
59. Swann NC, de Hemptinne C, Aron AR, Ostrem JL, Knight RT, Starr PA. Elevated synchrony in Parkinson disease detected with electroencephalography. *Ann Neurol*. 2015;78(5):742-750. doi:10.1002/ana.24507
60. Hwang BY, Salimpour Y, Tsehay YK, Anderson WS, Mills KA. Perspective: phase amplitude coupling-based phase-dependent neuromodulation in Parkinson's disease. *Front Neurosci*. 2020;14:558967. doi:10.3389/fnins.2020.558967
61. Little S, Brown P. Debugging Adaptive Deep Brain Stimulation for Parkinson's Disease. *Mov Disord*. Published online February 10, 2020:mds.27996. doi:10.1002/mds.27996
62. Little S, Pogosyan A, Neal S, et al. Adaptive deep brain stimulation in advanced Parkinson disease. *Ann Neurol*. 2013;74(3):449-457. doi:10.1002/ana.23951
63. Arlotti M, Marceglia S, Foffani G, et al. Eight-hours adaptive deep brain stimulation in patients with Parkinson disease. *Neurology*. 2018;90(11):e971-e976. doi:10.1212/WNL.0000000000005121
64. Gilron R, Little S, Perrone R, et al. Long-term wireless streaming of neural recordings for circuit discovery and adaptive stimulation in individuals with Parkinson's disease. *Nat Biotechnol*. Published online May 3, 2021. doi:10.1038/s41587-021-00897-5
65. Maidan I, Plotnik M, Mirelman A, Weiss A, Giladi N, Hausdorff JM. Heart rate changes during freezing of gait in patients with Parkinson's disease. *Mov Disord*. 2010;25(14):2346-2354. doi:10.1002/mds.23280

Figure legends

Figure 1 Electrode localization, experimental setup, and representation of the freezing index. (**A**) Localization of electrocorticography (ECoG) electrodes. The eight contacts (C1-C8) are visualized in the merged image of preoperative MRI and postoperative CT (left). C8 is the contact closest to the DBS bone hole. The white arrow points to the primary motor cortex. A reconstruction of the cortex and the eight contacts relative to the primary motor cortex (black arrow) is shown in the right figure. (**B**) Localization of the STN electrodes (white arrow) in the merged image of preoperative MRI and postoperative CT. (**C**) Experimental setup and protocol. Patients were asked to walk barefoot while completing a 10-meter (5 meters one way) back-and-forth timed up-and-go task at a self-selected pace with sensors attached to the lower limbs. The instant coordinates of the sensor were captured through an optoelectronic motion tracking system hanging on walls on both sides. Synchronized ECoG potentials were recorded through an extended cable. (**D**) The representative diagram of the freezing index (FI). The blue line represents the vertical position of the foot. The green line represents the forward position of the foot. The red line represents the FI. When the vertical kinematic rhythm becomes irregular and the forward motion stagnates, FI rises and exceeds the 3-point threshold (solid black line). Notably, if the FI drops below "3" but then rises back, with the lowest value still over "2" (gray dashed line), we consider this as one continuous freezing event rather than two. Thus, the diagram shows one continuous freezing event lasting from time point I to time point III. Because FI does not drop below "2", time point II does not mark the end of this freezing event.

Figure 2 Freezing trials have higher M1 PAC than nonfreezing trials. (**A**) Comodulograms showing group-level M1 beta-gamma PAC in rest standing (left), freezing (middle), and nonfreezing (right) trials. Deep colors indicate high PAC. (**B**) Box plots indicating the comparison of PAC between rest standing, freezing, and nonfreezing trials, which was tested using the Wilcoxon signed-rank test. The upper right plot shows the paired-comparison results. Each dot represents a patient. Dots landed above the gray dashed line have higher PACs in freezing trials ($PAC_{freezing}$). Dots landed below the gray dashed line have higher PACs in nonfreezing trials (PACnonfreezing). (**C**) Examples show the distributions of amplitude and preferred phase of the coupling in rest standing (red), freezing (orange), and nonfreezing trials (blue). These data are based on sub8, which is represented by the dot marked with a red dashed box in Figure 2B upper right plot. (**D**) Box plots comparing freezing time proportion, freezing frequency, and duration per freezing between dual-tasking

and no-task trials. (**E**) Box plots comparing PAC between dual-tasking and no-task conditions in all trials. (**F**) Box plots comparing PAC between dual-tasking and no-task conditions in nonfreezing trials. In box plots, the lower and upper borders of the box represent the 25^{th} and 75^{th} percentiles, respectively. The centerline represents the median. The whiskers extend to the smallest and largest data points that are not outliers (1.5 times the interquartile range). Significant *P* values after Bonferroni correction are indicated. $^{**}P < 0.01$, $^{*}P < 0.05$, signed-rank test.

Figure 3 Nonfreezing episodes in freezing trials also have higher PAC in M1. (**A**) Schematic diagram depicting the slicing of nonfreezing episodes (marked in orange, FN) and freezing episodes (marked in red, FF) in freezing trials. The blue line represents the vertical position of the foot, and the red line represents the freezing index (FI). (**B**) Schematic diagram depicting the slicing of normal-walking episodes (marked in blue, NN) in nonfreezing trials. (**C**) Violin plots indicate the comparison of relative PAC change between FN, FF, and NN episodes. The relative change was calculated as the percentage change with respect to NN scaling to the max value. Violin plots outline illustrate kernel probability density, with overlaid box plots using the same conventions as in Figure 2B. (**D**) A similar neurophysiological pattern that was characterized by higher M1 PAC in FN and FF episodes was presented in all subjects. $^{**}P < 0.01$, signed-rank test.

Figure 4 PAC during stable walking is correlated with freezing severity. (**A**) Distribution of condition-wise PACs during pre-walking standing (PAC_{stand}, left), stable walking (PAC_{stable} middle), and unstable walking ($PAC_{unstable}$ right). (**B**) Regression plots showing the correlation between PAC_{stand} and the freezing time proportion (upper), freezing frequency (middle), and duration per freezing (lower). (**C**) Regression plots showing the correlation between PAC_{stable} and the freezing time proportion (upper), freezing frequency (middle), and duration per freezing (lower). (**D**) Regression plots showing the correlation between $PAC_{unstable}$ and the freezing time proportion (upper), freezing frequency (middle), and duration per freezing (lower). Note, that each patient has three data points resulting in 14 x 3 PAC values (N = 42), as PAC was calculated in three stimulation conditions (i.e., HFS, LFS, and no-stimulation). Statistical dependence within subjects was accounted for using linear mixed-effects models. Significant correlations after Bonferroni correction are marked in red.

Figure 5 The reduction of PAC_{stable} predicts the improvement of freezing severity induced by DBS. (**A**) Box plots comparing PAC_{stand}, PAC_{stable}, and $PAC_{unstable}$ between no-

stimulation (NS) and stimulation (STIM) conditions. (**B**) Box plots comparing freezing time proportion, freezing frequency, and duration per freezing between NS and STIM conditions. Same conventions as in Figure 2B. $^{**}P < 0.01$, $^{*}P < 0.05$, signed-rank test. (**C**) Regression plots showing the correlation between the percentage change of PAC_{stand} and the percentage change of freezing time proportion (upper), freezing frequency (middle), and duration per freezing (lower). (**D**) Regression plots showing the correlation between the percentage change of PAC_{stable} and the percentage change of freezing time proportion (upper), freezing frequency (middle), and freezing duration (lower). (**E**) Regression plots showing the correlation between the percentage change of $PAC_{unstable}$ and the percentage change of freezing time proportion (upper), freezing frequency (middle), and duration per freezing (lower). Note, that each patient has two data points resulting in 14 x 2 PAC values (N = 28), as the reduction of PAC was calculated in two stimulation conditions (i.e., HFS and LFS). Statistical dependence within subjects was accounted for using linear mixed-effects models. Significant correlations after Bonferroni correction are marked in red. %RD = percentage reduction; %IMP = percentage improvement.

Figure 6 STIM trials have lower freezing severity than NS trials even when under similar levels of PAC. (**A**) The distribution of PAC in no-stimulation (NS) and stimulation (STIM) trials. Trials with PACs between 0 and 0.4 in both the NS and STIM groups were picked out as PAC-matched trials (marked by yellow-shadow background) for further analyses. Box plots showing the (**B**) comparison of PAC, (**C**) comparison of freezing time proportion, (**D**) comparison of freezing frequency, and (**E**) comparison of duration per freezing between PAC-matched NS and STIM trials. Same conventions as in Figure 2B. $^{**}P < 0.01$, $^{*}P < 0.05$, signed-rank test. ns = not significant.

Figure 7 A graphical representation of the proposed "bandwidth model" of FOG. Three main elements constitute the model: (I) the baseline occupation, (II) the dynamic fluctuation, and (III) the bandwidth limit. The X-axis represents the time axis, and Y-axis represents the occupied bandwidth. When baseline occupation plus dynamic fluctuation exceeds the bandwidth limit, freezing occurs. Baseline occupation can be quantified through M1 PAC. In the OFF-stimulation state (left), the baseline occupation (M1 PAC) maintains at a high level, leading to a high probability of exceeding the bandwidth limit. In the ON-stimulation state (right), a reduction of baseline occupation and an elevation of bandwidth limit clean up larger available bandwidth that can be used to process dynamic fluctuation, leading to a lower probability of freezing.

Table 1 Demographics of the 16 FOG patients

Patient	Age/gender	DD (years)	LEDD	FOGQ	MDS-UPDRS [a]	MDS-UPDRS [b]	MDS-UPDRS [c]	HFS voltage (V) [d]	LFS voltage (V) [e]	Stimulation contacts
Sub1	72/F	10	675	10	47	28	24	3.0	3.3	2-4+, 6-8+
Sub2	60/F	7	750	20	47	24	31	2.5	2.7	2-4+, 6-8+
Sub3	57/F	5	375	14	49	24	34	2.7	2.7	2-4+, 6-8+
Sub4	66/F	10	513	21	61	22	42	2.8	2.8	2-4+, 6-8+
Sub5	53/M	12	1100	24	79	25	31	2.1	1.8	3-1+, 7-5+
Sub6	70/M	12	688	17	70	37	28	2.8	2.8	2-4+, 6-8+
Sub7	73/F	9	1439	20	51	27	46	2.1	2.1	4-3+, 8-7+
Sub8	67/F	6	500	22	52	30	26	3.0	3.2	2-4+, 6-8+
Sub9	59/F	9	700	16	46	21	11	2.8	2.8	2-4+, 6-8+
Sub10	78/M	5	550	18	58	24	27	2.2	2.2	1-3+, 5-7+
Sub11	76/M	8	1351	13	41	11	10	3.0	3.2	2-4+, 6-8+
Sub12	66/F	15	669	13	55	8	21	3.5	3.5	2-4+, 6-8+
Sub13	61/M	7	1150	22	37	18	22	2.4	3.5	4-1+, 8-5+
Sub14	66/F	15	925	20	39	20	27	2.3	2.3	4-2+, 8-6+
Sub15	67/M	10	913	16	42	20	10	2.5	2.5	2-4+, 6-8+
Sub16	67/F	9	1000	15	27	5	13	3.0	3.5	1-3+, 6-8+

FOG: freezing of gait; DD: disease duration; LEDD: levodopa equivalent daily dose; FOGQ: freezing of gait questionnaire; MDS-UPDRS: MDS-Unified Parkinson's Disease Rating Scale; HFS: high frequency stimulation; LFS: low frequency stimulation.

[a] Baseline off-medication score.

[b] Baseline on-medication score.

[c] One month postoperative on-stimulation off-medication score.

[d] Stimulation frequency and pulse width for high frequency stimulation: 130 Hz and 60 μs.

[e] Stimulation frequency and pulse width for low frequency stimulation: 60 Hz and 60 μs.

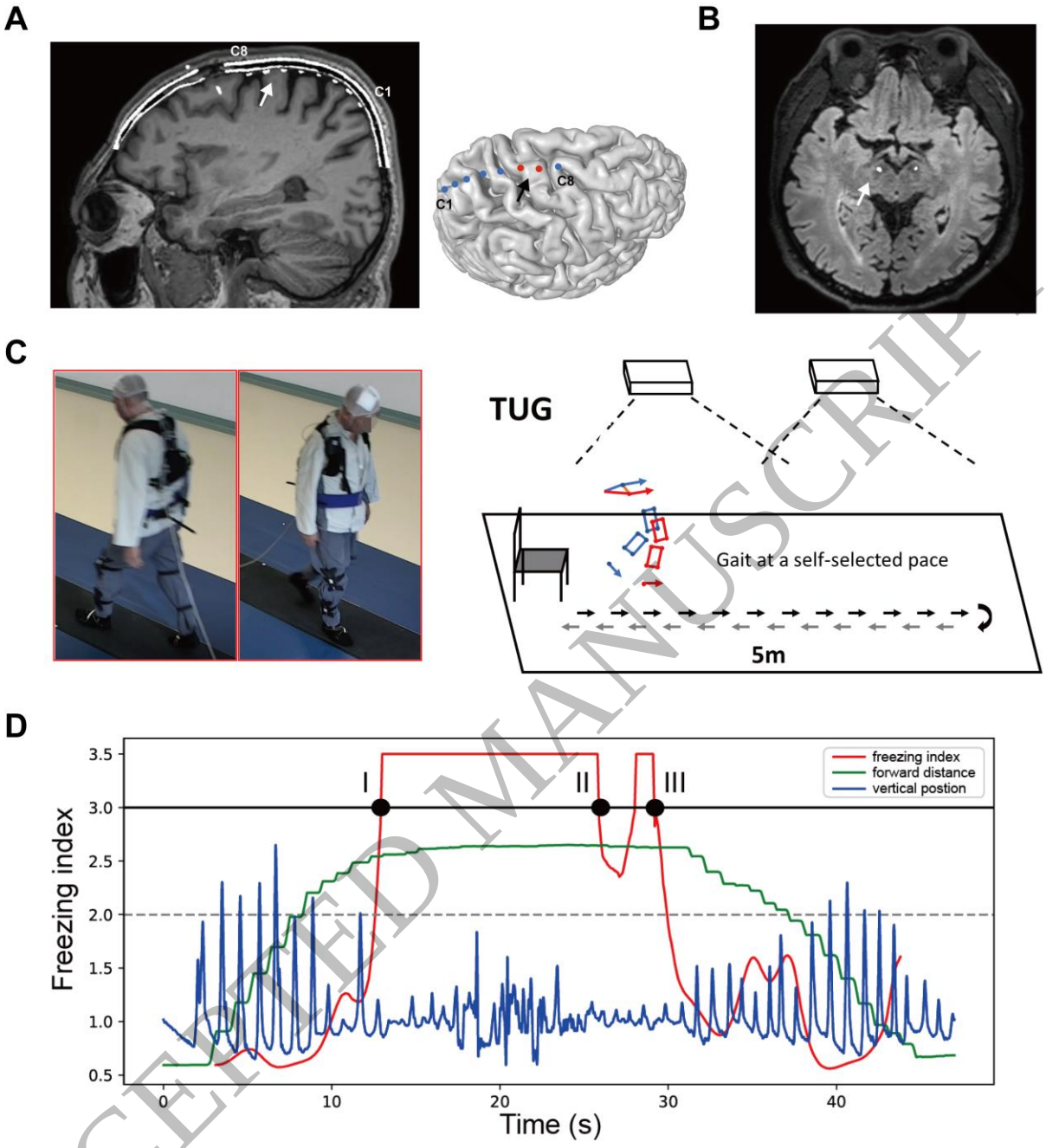

Figure 1
159x174 mm (3.8 x DPI)

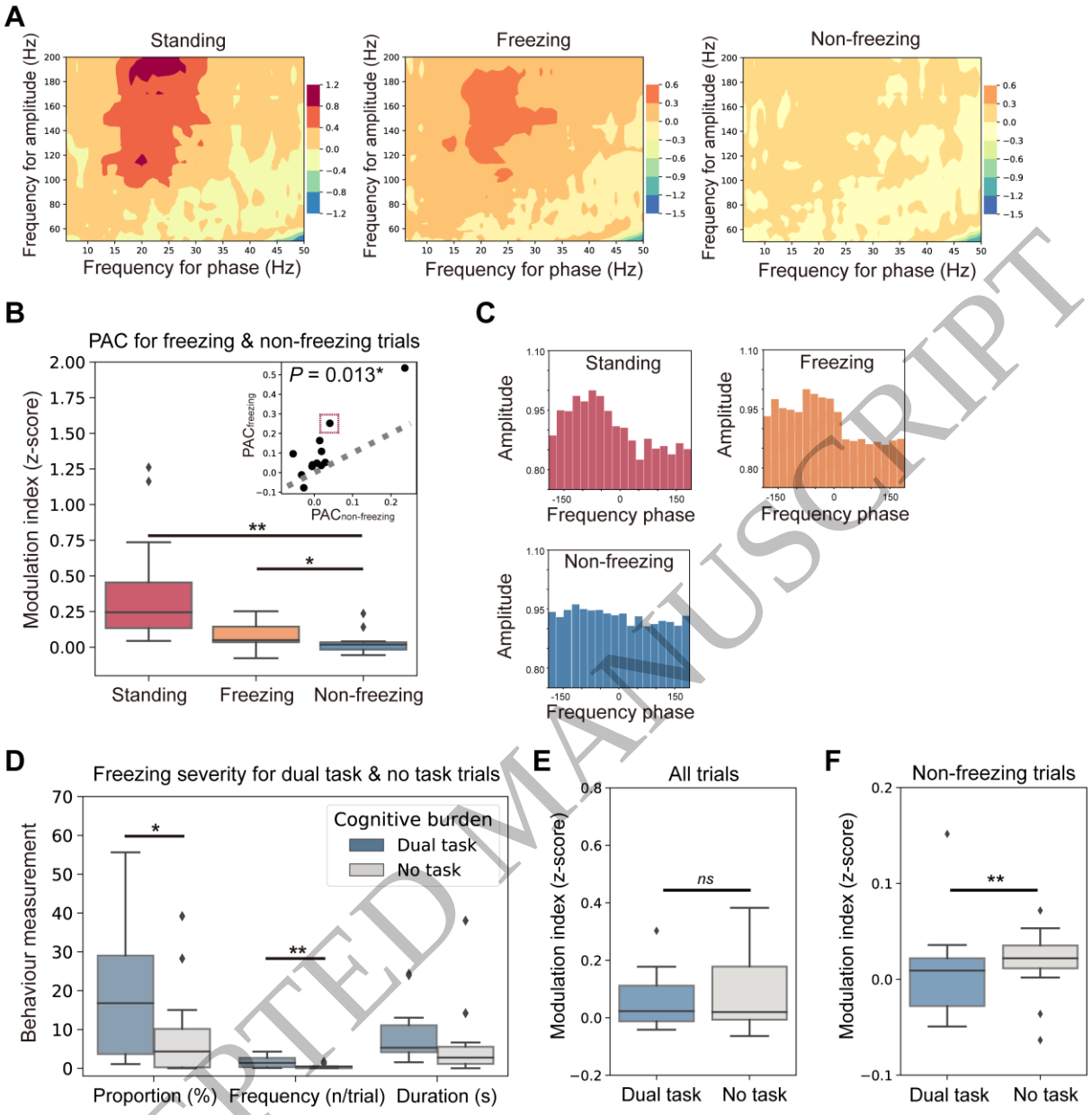

Figure 2
159x163 mm (3.8 x DPI)

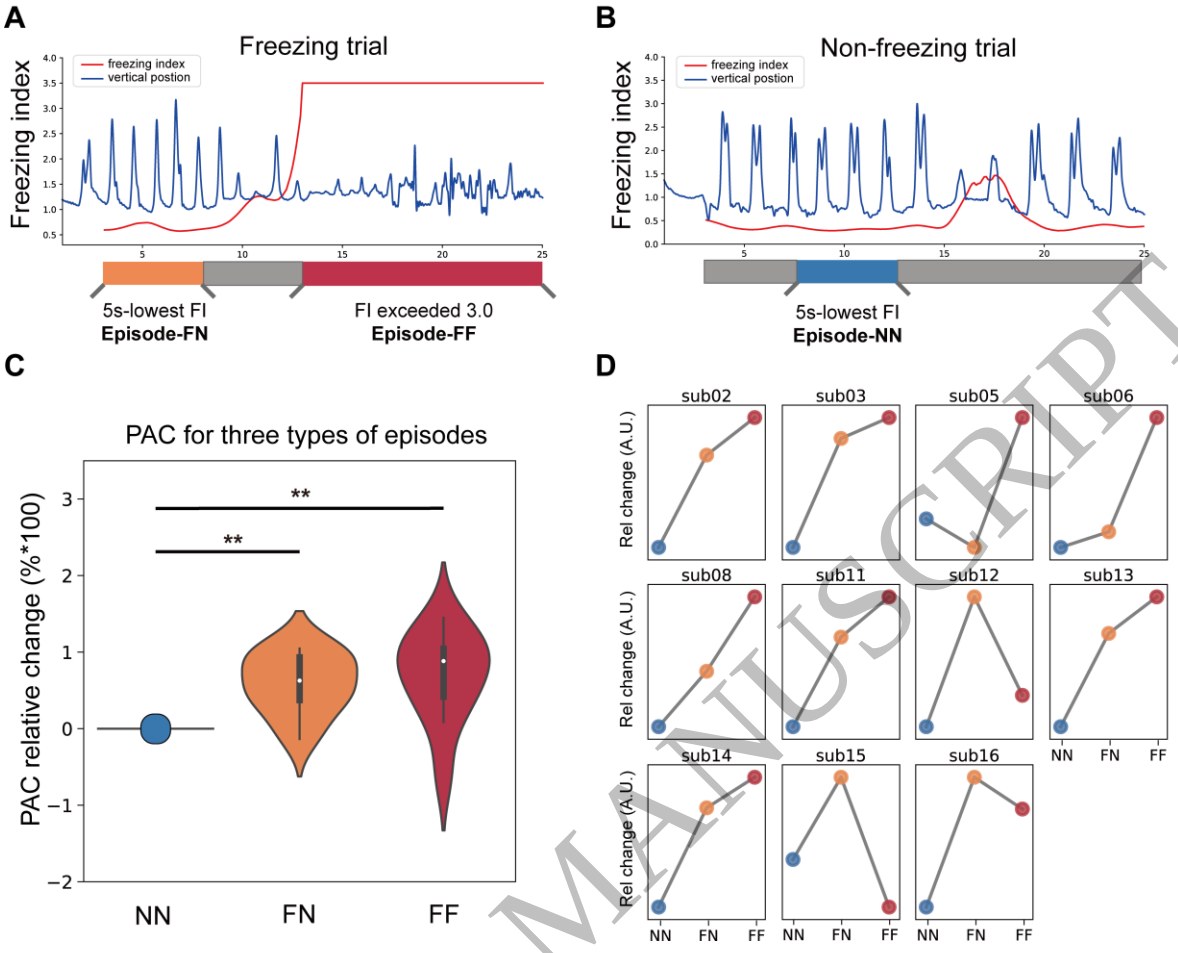

Figure 3
159x124 mm (3.8 x DPI)

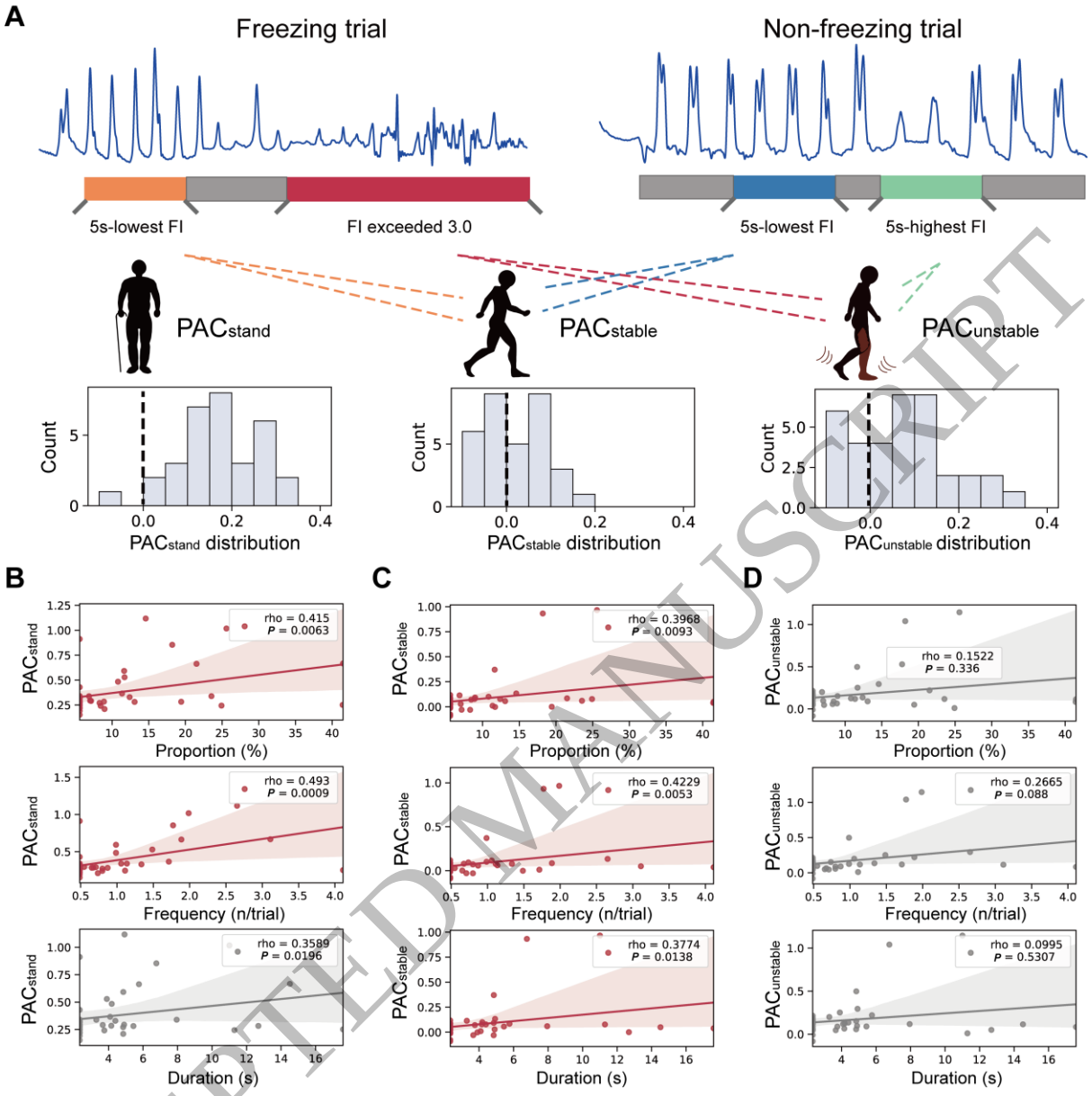

Figure 4
159x160 mm (3.8 x DPI)

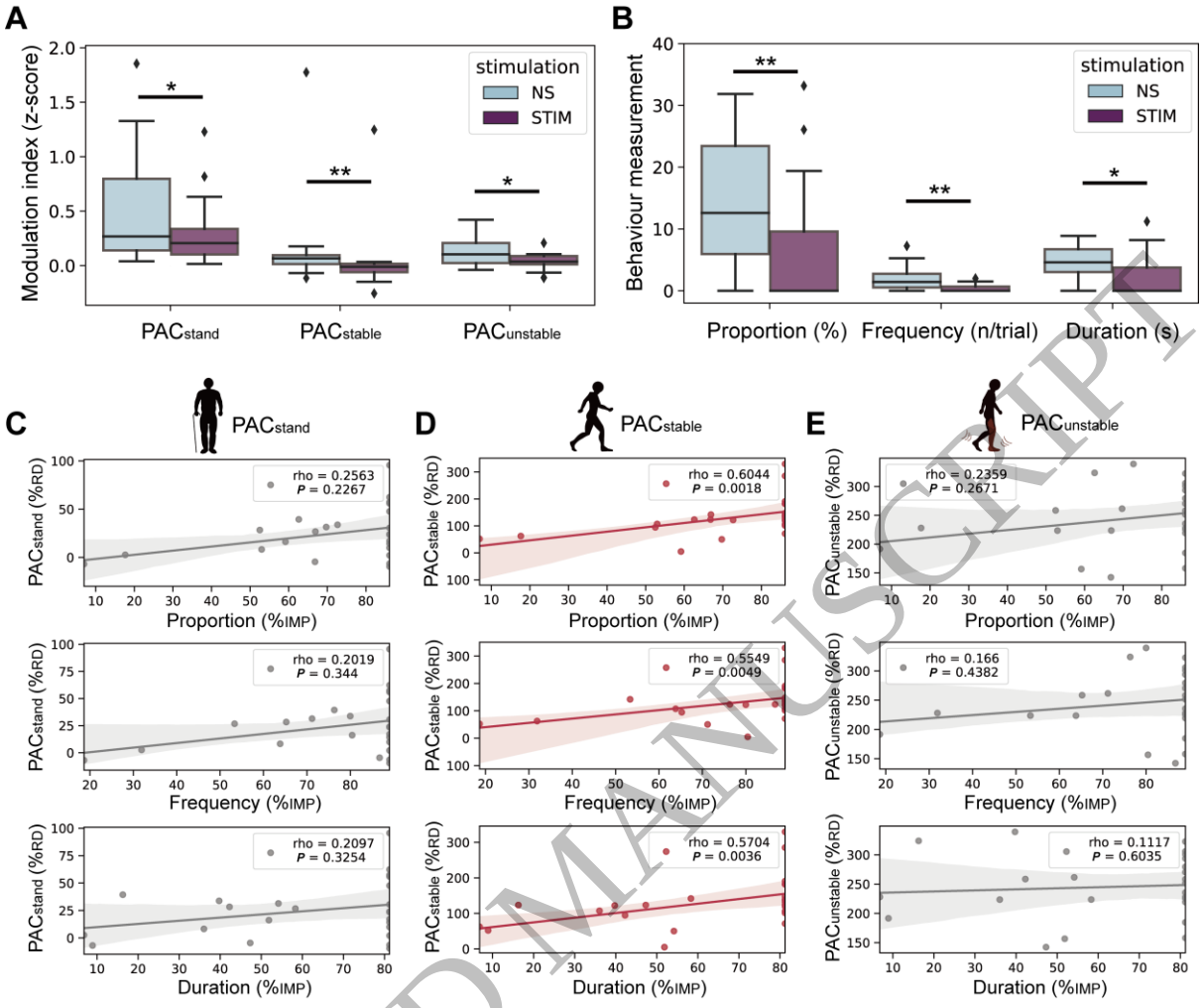

Figure 5
159x133 mm (3.8 x DPI)

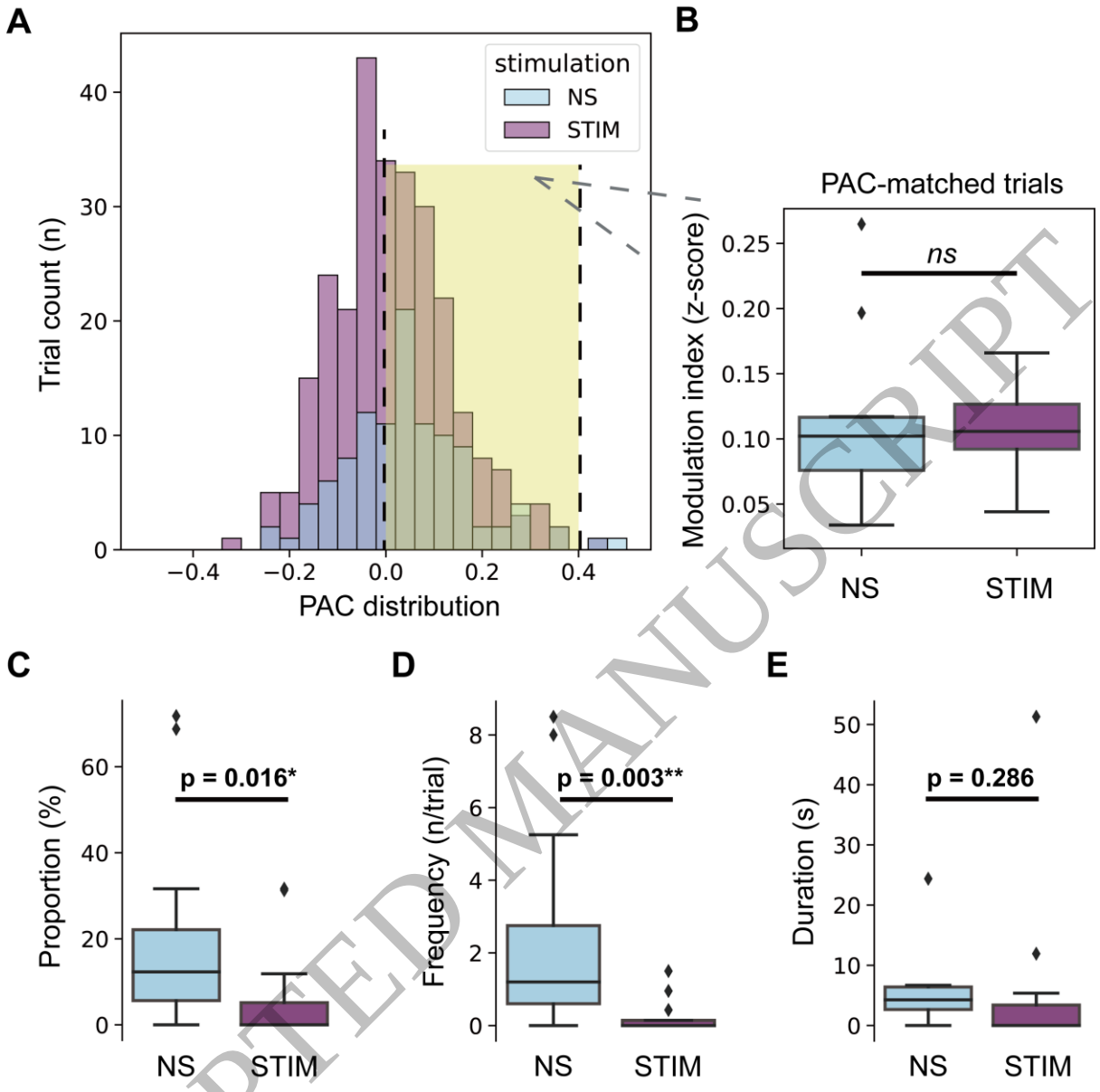

Figure 6
159x158 mm (3.8 x DPI)

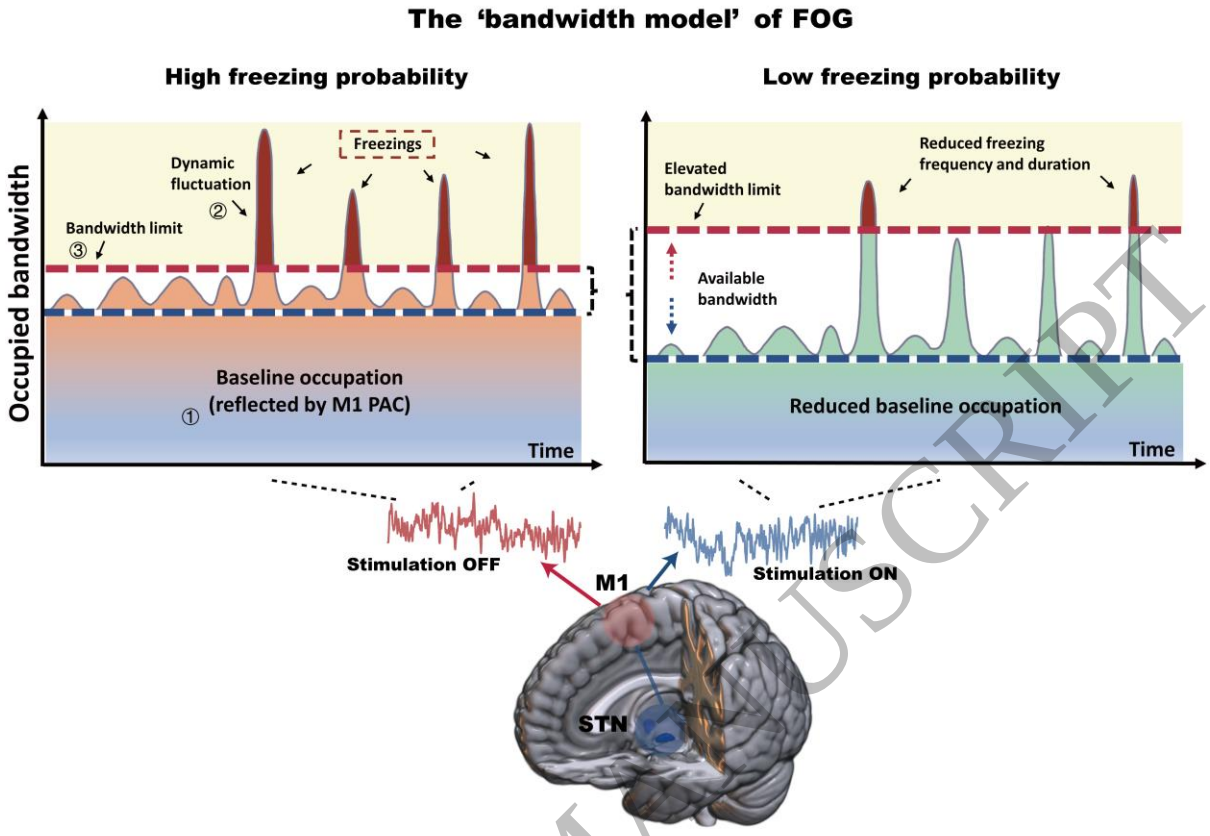

Figure 7
159x113 mm (3.8 x DPI)